Int. J. Electrochem. Sci., 12 **(2017)** 5951 – 5963, doi: 10.20964/2017.07.77

International Journal of
ELECTROCHEMICAL
SCIENCE
www.electrochemsci.org

Co-modified Commercial P25 TiO_2 by Fe Doping and g-C_3N_4 Coating as High Performance Photocatalyst under visible light irradiation

Yao Fang[1], *Yongkui Huang*[1], *ZhiJiang Ni*[1], *ZhiLei Wang*[1], *Shifei Kang*[2,*], *Yangang Wang*[2,*], *Xi Li*[1,*]

[1]Department of Environmental Science and Engineering, Fudan University, Shanghai 200433, China
[2]School of Environment and Architecture, University of Shanghai for Science and Technology, Shanghai 200093, China
[*]E-mail: xi_li@fudan.edu.cn, sfkang@usst.edu.cn

Received: 27 April 2017 / *Accepted:* 24 May 2017 / *Published:* 12 June 2017

The g-C_3N_4-coated and Fe-doped TiO_2 visible-light-driven photocatalysts were synthesized by a simple mixing method combined with calcination process, in which the commercial Degussa P25 TiO_2 was used as a titanium source. The new photocatalysts were investigated by X-ray diffraction, transmission electron microscopy, X-ray photoelectron spectroscopy, ultraviolet-visible diffuse reflection spectroscopy, scanning electron microscopy, and Fourier transform infrared spectroscopy. The co-presence of uniform g-C_3N_4 coating layers and doped metal ions was proved and the visible light absorption was significantly enhanced after modification. The photocatalytic efficiency and stability of the new photocatalysts in degradation of dyes and Cr(VI) under visible-light irradiation were remarkably enhanced, and were mainly dependent on the ratio of g-C_3N_4 and metal ions. Based on the electrochemical impedance spectroscopy results, we believe the interfacial effect between g-C_3N_4 and TiO_2 and the doping Fe ions in the heterojunction could improve the separation and transfer of photo-induced charge carriers and thereby enhanced the photocatalytic performance.

Keywords: TiO_2; g-C_3N_4; Fe-doping; heterojunction; photocatalyst

1. INTRODUCTION

Environmental pollution has been intensified and thus critically threatens the economic and social development of humans. In particular, wastewater effluents, such as the dyestuffs and heavy-metal ions, have become the key issues as they cannot be effectively treated by traditional processing technics. Under this circumstance, the development of novel efficient techniques becomes increasingly significant worldwide. A research hotspot is the photocatalytic degradation technique based on TiO_2 semiconductor, owing to the utilization of environmental-friendly solar energy resource[1, 2]. TiO_2 has been widely used in photocatalytic works owing to its advantages of low-cost, physiochemical stability

and non-toxicity. However, with a large bandgap energy of 3.2 eV, TiO_2 could only be motivated by UV light and only takes up about 4% of sunlight. In this instance, much efforts have been made to obtain high active visible-light-driven photocatalysts through efficient modification of TiO_2, including semiconductor coupling, doping with metals or nonmetals, and deposition with noble nanoparticles.

Recently, graphite phase carbonic nitrogen (g-C_3N_4), a graphite-analogous metal-free semiconducting photocatalyst with a medium bandgap (2.7 eV) and many advantages (e.g. high thermal stability, conspicuous visible-light absorption and peculiar electronic structure), has attracted the photocatalytic research field[3-5]. Meanwhile, with the composition of only carbon and nitrogen, g-C_3N_4 can be easily prepared from nitrogen-rich compounds, such as melamine. On account of its conjugative structure, g-C_3N_4 has a high ability of photogenerated charge separation, and thus is considered to be an ideal candidate for the design of photocatalytic compound materials[6-9]. In addition, the presence of metal ion dopants in semiconductors notably improves the photocatalytic performance by increasing the visible-light absorption and prolonging the lifetime of photoinduced charge carriers. Many efforts have been devoted to synthesis of efficient visible-light-driven transition metal-doped emiconductor photocatalysts, and confirm that Fe is one of the optimal choices[10-13]. Therefore, it has been planned to prepare TiO_2 photocatalysts with the joint modification of g-C_3N_4 coupling and Fe ion doping. However, most of the existing methods are complex and involve expensive raw materials or cause environmental problems, such as by-product pollution[14].

Regarding the commercial potential of modified TiO_2 photocatalysts, the use of cheap raw materials is also the great concern in the research fields of materials chemistry and environmental engineering. Among all the commercial TiO_2 materials, the most attractive candidate is Degussa P25 TiO_2 with average particle size of 21 nm and surface area of 50 m^2/g produced by Degussa Corp.. P25 nanoparticles possess effective photocatalytic activity due to their unique mixcrystal structure of 80% anatase and 20% rutile. However, pure P25 TiO_2 cannot use visible light, which significantly restricts its practical applications. Therefore, the joint modification of g-C_3N_4 coupling and Fe doping, which can improve the visible-light-driven activity of P25 TiO_2, was proposed for construction of high-performance photocatalysts.

In this work, a series of modified P25 photocatalysts were prepared through a facile approach by mixing different contents of P25, melamine and $Fe(NO_3)_3 \cdot 9H_2O$ together, followed with a calcination process at 550 ℃. The physicochemical properties of the photocatalysts were investigated, and the photocatalytic activity and stability were measured with photodegradation tests on dyes and Cr(VI) under visible light irradiation[15]. A potential mechanism underlying the enhancement of photocatalytic performance was proposed.

2. EXPERIMENTAL

2.1. Materials

All chemicals used here were of analytical grade and employed without further purification. All materials were purchased from Shanghai Chemical Corp., Ltd., except TiO_2 (Degussa(P25) Corp.). Deionized water was used throughout the experiements.

2.2. Preparation of Fe-doped and g-C_3N_4-coated P25 composites (Fe-CN-P25)

Fe-CN-P25 composites were synthesized with a facile route. Firstly, 0.5 g of P25, 0.01 g of $Fe(NO_3)_3 \cdot 9H_2O$ and a certain amount of melamine (1-10 g) were added into deionized water under stirring at room temperature. The resulting suspensions were placed in an oven and heated to 80 ℃, which removed the water. After that, the dried solid mixtures were removed to a muffle furnace and calcined at 550 ℃ for 4 h at a rate of 5 ℃ min^{-1}. After natural cooling down, the final products were grinded as powder and labeled as PCNFx, where x is the weight of melamine (for example, PCNF1 is prepared by 1g melamine). Meanwhile, to study the role of metal content on the photodegradation activity of Fe-CN-P25, we prepared another series of photocatalysts under the same conditions, except that the amount of $Fe(NO3)_3 \cdot 9H_2O$ was changed from 0.005 to 0.02 g and the dosage of melamine was 5 g. The products were denoted as PFCNx, where x is the mass percent of $Fe(NO_3)_3 \cdot 9H_2O$ to P25 (1%-4%). For comparison, pure g-C_3N_4 was prepared under the same steps without addition of P25 or metal.

2.3. Characterization

The crystal structures and phase purity of the photocatalysts were investigated on an X-ray diffractometer (XRD, Rigaku D/Max2rB; Cu-Kα radiation, λ=1.5406 Å, scanning rate = 0.02 °s^{-1}). Their morphologies and compositions were characterized on an FEI XL-30 scanning electron microscope (SEM) and a JEOL-JEM2010 transmission electron microscope (TEM) at the acceleration voltages of 25 and 200 kV, respectively. Other instruments included a UV-2600 ultraviolet-visible (UV-Vis) absorption spectrophotometer (Japan), and a Nicolet Nexus 470 FTIR Fourier transform infrared (FT-IR) spectrometer. The oxidation states of C, N, O, Ti and Fe on the surfaces of the composites were explored on a PHI 5000 C ESCA X-ray photoelectron spectroscope (XPS) with Al Kα as the exciting source. The electrochemical impedance spectroscopy (EIS) was recorded by a Chi660e electrochemical workstation based on a conventional three-electrode systemwitha frequency range from0.01 Hz to 100 kHz atthe circuit potential.

2.4. Photocatalytic activity for degradation of dye and Cr(VI)

Dyes [Rhodamine B (RhB), methyl orange (MO)] and toxic Cr(VI) were selected to evaluate the visible-light-driven activities of the new photocatalysts. Each time, a photocatalyst (50 mg) was dissolved in a RhB/MO solution (50 mL, 10 mg/L) or Cr(VI) solution (50 mg/L). Prior to the experiment, the Cr(VI) solution was adjusted with $HClO_4$ to pH 2~2.5 and ethylene diamine tetraacetic acid (EDTA) was added as a sacrificial reagent. A 300W Xe arc lamp with a UV-cutoff filter (420 nm) provided the simulative visible light. Appropriate temperatures were maintained by cooling water circulation pumps that were connected to the reactor. Photocatalytic reaction was proceeded a 100 mL cylindrical quartz vessel under stirring. The suspensions were placed in the dark for 30 min to reach a desorption/adsorption balance. Then the suspensions were collected at given time interval (each 1 mL), diluted with deionized water, and speedily centrifuged, which separated the solids from the solution.

The RhB (or MO) concentration was measured by the UV-Vis spectrophotometer at λ=550 nm (or 464 nm), while the Cr(VI) concentration was detected at λ=540 nm based on a DPC developer method[16].

3. RESULTS AND DISCUSSION

3.1. XRD

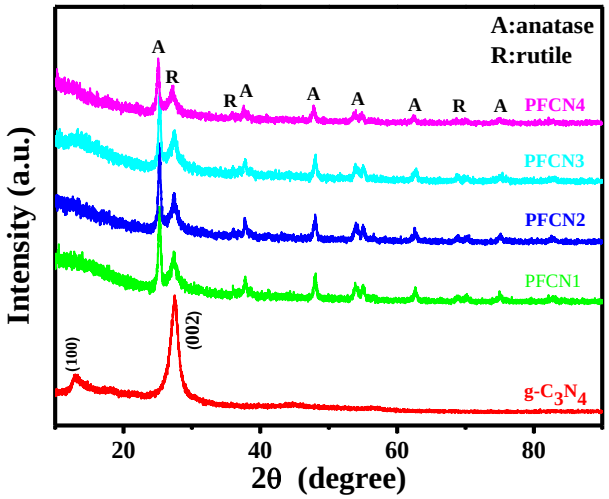

Figure 1. XRD patterns of g-C_3N_4 and PFCNx.

Figure 1 shows the typical XRD patterns of g-C_3N_4 and the PFCNx. The pure g-C_3N_4 exhibits two distinct diffraction peaks at 13.2° and 27.3°, corresponding to the (101) and (002) crystal planes, respectively. All PFCNx show a series of peaks marked with A and R. Specifically, the "A" peaks with 2θ = 25.4° (101), 37.8° (004), 48.2° (200), 54.5° (105) and 62.8° (204) correspond to the crystal faces of anatase TiO_2 (JCPDS card No.21-1272), while the "R" peaks at 2θ =27.2°, 36.1° and 69.7° can be indexed to the rutile TiO_2 (JCPDS card No.21-1276)[17-19]. The XRD patterns of PFCNx rarely changed after coating with g-C_3N_4, because the main peak of g-C_3N_4 in 27.3° and the rutile-phase diffraction peak of TiO_2 in 27.2° were partly overlapped and the g-C_3N_4 had low XRD intensity. Meanwhile, no obvious diffraction peak of doped-metal appeared because of the low content of Fe^{3+} (<5 wt.%). In comparison, the peaks of anatase TiO_2 were relatively weakened after the addition of metal content. The XRD patterns prove the high purity, stable crystal forms and hybrid heterojunction in the photocatalysts prepared here[10, 20].

3.2. Morphology

The morphology and microstructure of some representative photocatalysts were investigated by SEM and TEM. As shown in Fig. 2a and 2b, the PFCN2 exhibits uniform pore size distribution, and numerous TiO_2 nanoparticles disperse on the surfaces of the disordered g-C_3N_4. This remarkable connection proves the successful combination of TiO_2 and g-C_3N_4 and may contribute to the isolation of photoinduced electron-hole pairs. The combination details of PFCN2 characterized by TEM and

HR-TEM are showed in Fig. 2c-f. Clearly, TiO_2 particles are in intimate interfacial contact with a moderate amount of multilayer g-C_3N_4 (Fig. 2c-e). The HR-TEM image (Fig. 2f) obtained from Fig. 2e indicate the principal lattice fringe of d=0.35 nm corresponds to the (101) plane of anatase TiO_2, which is consistent with the XRD results[17, 21].

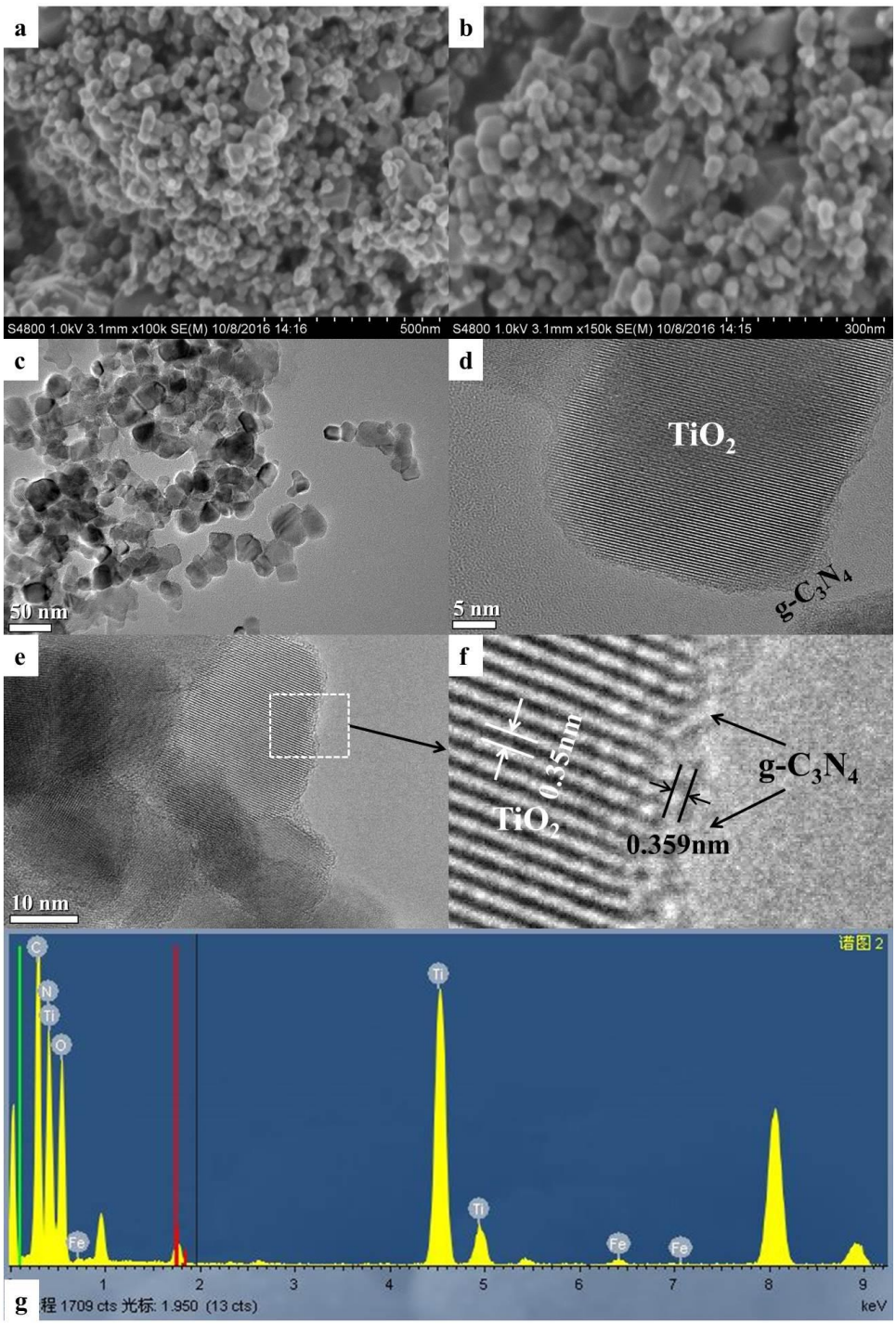

Figure 2. SEM images (a, b), TEM images (c-f) and EDS pattern (g) of PFCN2.

Meanwhile, TiO_2 nanoparticles are mostly surrounded by a few g-C_3N_4 layers whose average monolayer thickness is about 0.359 nm (Fig. 2f). Furthermore, the energy dispersive spectrometer (EDS) pattern (Fig. 2g) shows the products are composed of C, N, O, Ti and Fe, which is consistent with the preparation scheme. The interfacial contact in the heterojunction composites may drive the photoinduced electrons to transfer from g-C_3N_4 to TiO_2[22, 23]. Thus, as expected, the photodegradation activity of the new photocatalysts under visible light was enhanced.

3.3. UV-vis diffuse reflection spectroscopy (DRS)

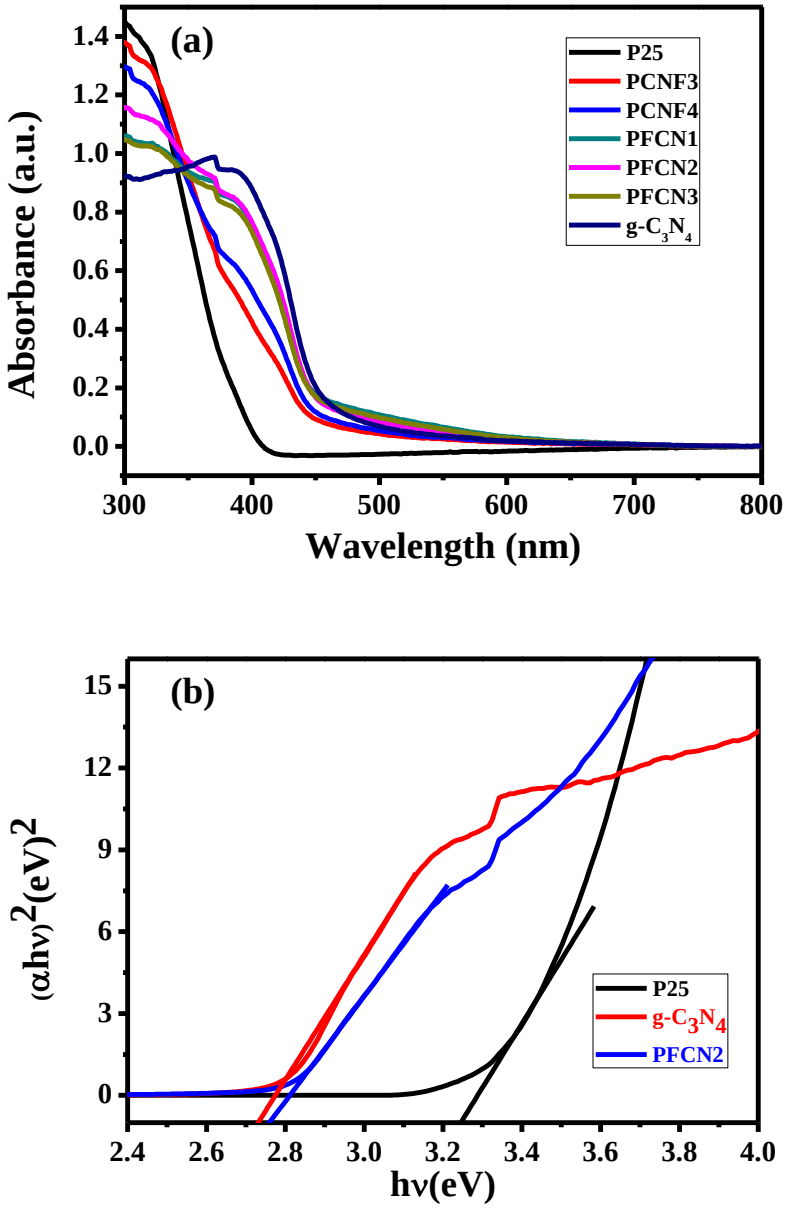

Figure 3. (a) UV-vis DRS spectra of P25, g-C_3N_4 and Fe-CN-P25 composites; (b) Plots of $(\alpha h\nu)^2$ vs. energy ($h\nu$) of P25, g-C_3N_4 and PFCN2 sample.

The optical properties of P25, pure g-C_3N_4 and composite photocatalysts were explored with a UV-vis DRS meter. As showed in Fig.3 (a), P25 almost only absorbed ultraviolet light with a sharp edge at about 400 nm, while pure g-C_3N_4 responded actively in the visible light region up to λ=460 nm. Furthermore, all PFCNx and PCNFx could absorb more significantly at λ >400 nm compared with P25, and the absorption ability increased with the mass degree of g-C_3N_4 in the composite. The plots of $(\alpha h\nu)^2$ vs. energy (hν) in Fig. 3(b) show that the band gap energies of P25 and g-C_3N_4 were estimated to be 3.24 and 2.73 eV, respectively, which are nearly consistent with the literature[24, 25]. After coupling with g-C_3N_4, the PFCN2 showed the most efficient visible light absorption and its band gap energy was about 2.76 eV. The UV-vis spectra further confirm the tight interfaces between P25 and g-C_3N_4, and it is expected the catalyst with lower band gap energy has a higher visible-light photocatalytic ability.

3.4. FT-IR spectra

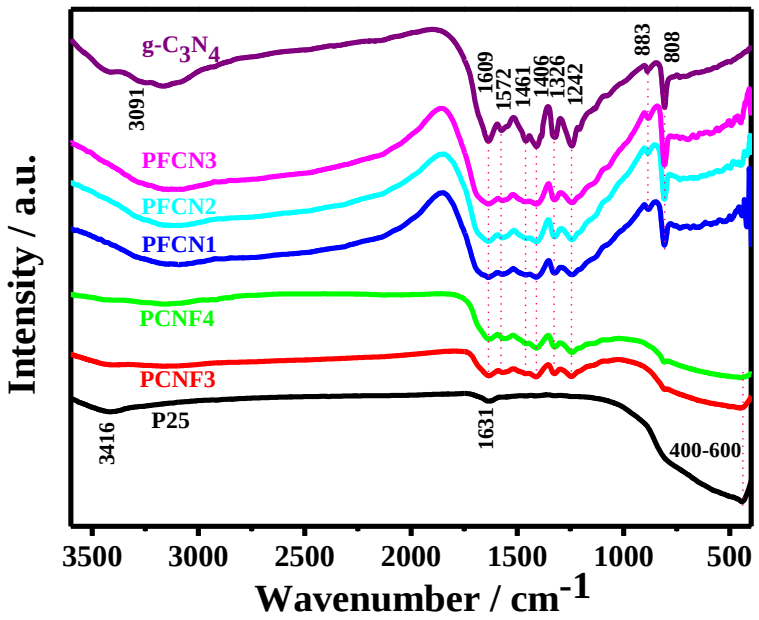

Figure 4. FT-IR spectra of P25, g-C_3N_4 and Fe-CN-P25 composites.

To further determine the existence of g-C_3N_4 and study its interaction with P25, we tested the FT-IR spectra of some representatives (Fig. 4). Clearly, P25 shows a broad peak at around 400-600 cm^{-1} (stretching modes of Ti-O and Ti-O-Ti) and two broad peaks at around 3400 and 1630 cm^{-1} (attributed to the surface hydroxyl groups and surface-adsorbed water, respectively). Additionally, the pure g-C_3N_4 shows the strong peaks within 1240-1650 cm^{-1} (typical stretching vibration modes of C-C and C@N heterocycles) and two peaks at around 808 and 3000-3400 cm^{-1} (breathing vibration of heptazine rings and stretching vibration of N-H, respectively)[16, 18, 26]. PFCNx and PCNFx also show the main typical peaks of g-C_3N_4 and P25, which is reasonable of the hybridization of g-C_3N_4 and

P25. It should be noted that with the increasing degree of g-C_3N_4, the peaks related to g-C_3N_4 are continuously strengthened while the peaks assigned to P25 are weakened. These vibration trends reflect the hybridization degree and may modestly influence the photocatalytic performance.

3.5. XPS

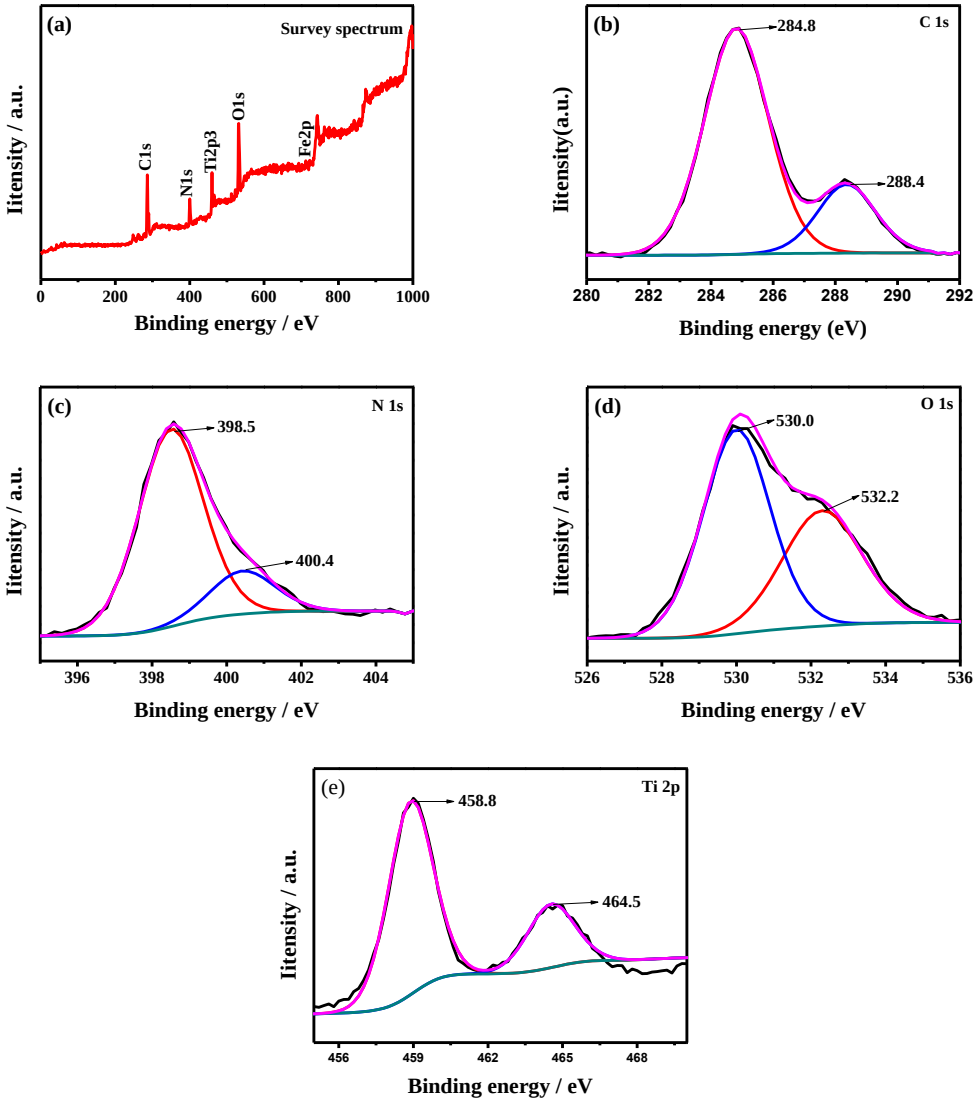

Figure 5. XPS spectra of PFCN2: survey scan spectrum (a), high-resolution spectra of C 1s (b), N 1s (c), O 1s (d) and Ti 2p (e).

The chemical states of surface elements in the representative PFCN2 were analyzed by XPS. The survey spectrum in Fig.5a clearly indicates that PFCN2 is composed of C, N, Ti, O and Fe. It also proves the photocatalyst has high purity without other peak, which is consistent with the EDS pattern in Fig. 2. The high-resolution C 1s spectrum in Fig. 5b shows that PFCN2 has two C 1s peaks at 284.8 and 288.4 eV, respectively. The former strong peak is assigned to the C–C coordination of the XPS

instrument and the sp^2 C–C in g-C_3N_4, while the latter one is attributed to sp^3-bonded carbon of C–N in g-C_3N_4 (literature)[27]. The N 1s spectrum shows two peaks with binding energy of 398.5 and 400.4 eV, respectively, which are attributed to the sp^2-hybridized nitrogen group (C=N–C) and tertiary nitrogen N–C_3 group, respectively[18]. The high-resolution spectrum of O 1s shows the two typical peaks with binding energy of 530.0 and 532.2 eV, respectively (Fig. 5d), which are ascribed to the Ti–O band of the anatase TiO_2 and the surface –OH group, respectively. The HR XPS spectra show two Ti 2p peaks at 458.8 and 464.5 eV, respectively (Fig. 5f), which can be attributed to Ti $2p_{3/2}$ and Ti $2p_{1/2}$ of Ti^{4+} in TiO_2, respectively[20, 21]. All these results confirm the heterojunction of TiO_2 and g-C_3N_4 with Fe-doping in the composites as-prepared.

3.6. Photocatalytic activity

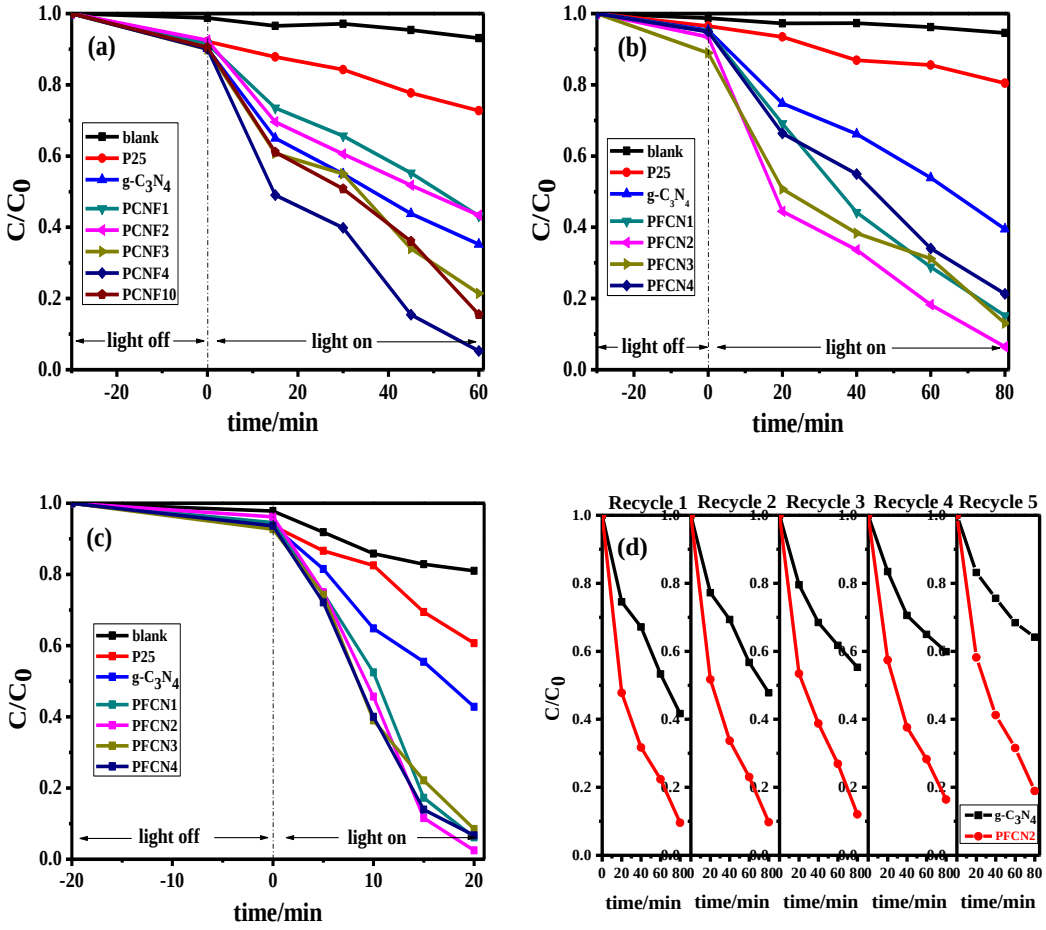

Figure 6. Photocatalytic activity of P25, g-C_3N_4, and Fe-CN-P25 composites for photodecomposition of (a) RhB, (b) MO and (c) Cr(VI) in solutions (a/b. 10 mgL^{-1}, c.50 mgL^{-1}) under visible-light irradiation; The recycling performance the of the photocatalyst in photodegradation of MO (d).

The photocatalytic activities of the samples evaluated by the degradation tests of dyes and Cr(VI) under visible-light irradiation are showed in Fig. 6. The RhB solution was kept in dark for 30 min in advance to reach the adsorption-desorption balance, where C_0 is the initial concentration of the RhB solution and C is the actual concentration measured at specific time (Fig. 6a). The blank tests indicate that RhB and MO were both stable, so the photolysis could be neglected (Fig. 6a-b). Meanwhile, after 1 h of reaction, the RhB removal efficiencies of P25, g-C_3N_4, PCNF1, PCNF2, PCNF3, PCNF4 and PCNF10 were 27.3%, 64.8%, 56.8%, 56.6%, 78.6%, 94.9% and 84.5%, respectively, indicating that the Fe-CN-P25 composites all have much higher photodegradation activity than pure P25 and g-C_3N_4. The degradation efficiencies first increased (from PCNF1 to PCNF4) and then all decreased with further increase of g-C_3N_4 content, indicating the addition of excessive g-C_3N_4 could restrain the photocatalytic performance. The possible reasons are that the increase of g-C_3N_4 content could modestly promote the visible light absorption, thus forming more electron-hole pairs, and also improve the transfer and separation of photoinduced charge carriers. However, further increase of g-C_3N_4 content leads to an inappropriate ratio between g-C_3N_4 and P25, while the addition of excessive g-C_3N_4 may act as the recombination center of electrons and holes, because of its narrow bandgap. In addition, the low content of P25 nanoparticles also reduces the formation of activated sites and thereby restricts the transfer of photogenerated electrons from the surface of g-C_3N_4 to P25, leading to a poor photocatalytic activity under visible light irradiation. Furthermore, Fig. 6(b) shows the MO photodegradation tests of several samples under visible-light irradiation. Clearly, the degradation rates of all samples in 80 min rank as follows: PFCN2 > PFCN3 > PFCN1 > PFCN4 > g-C_3N_4 > P25. In other words, PFCN2 doped with 2% Fe^{3+} shows the highest MO removal efficiency (88.6%) under visible-light, indicating that the optimal Fe^{3+} doping content is about 2%. The photocatalytic performance in degradation of Cr(VI) is shown in Fig. 6(c). Clearly, after 20 min of reaction, the Cr(VI) degradation efficiencies of blank test, P25 and g-C_3N_4 are 18.9%, 39.3% and 57.2%, respectively. Compared with photodecomposition of MO, the removal effects of different modified samples were inconspicuous as the degradation efficiencies of PFCN1-4 were all close to 95%, which means a highly increased photocatalytic activity in degradation of Cr(VI). The stability of PFCN2 was investigated by reusing the samples after MO photodegradation tests (Fig. 6d). Notably, the photocatalytic activity of PFCN2 was not reduced significantly after 5 consecutive cycles of MO photodegradation compared with pure g-C_3N_4. It is suggested the g-C_3N_4-P25 heterojunction could improve the photocatalytic stability, which is very important for the application of wastewater treatment[16, 28]. All these results indicate the photocatalysts have high activity and cycling stability in degradation of dyes and Cr(VI) under visible-light irradiation.

3.7. Electrochemical properties of Fe-CN-P25 photocatalysts

Electrochemical impedance spectroscopy (EIS) was conducted to explore the photoinduced charge separation of the samples (Fig. 7). Normally, The EIS Nyquist plots can be divided to a semicircle segment and an inclined line segment, while the resistance of the semicircle is ascribed to the charge transfer process. As reported, a smaller arc radius of the EIS Nyquist plot means the

interfacial charge transfer is faster and the separation of photoinduced electron-hole pairs is more effective[6, 29]. As shown in Fig. 7, PFCN2 has a smaller arc radius of EIS Nyquist plot than pure g-C_3N_4, which suggests the separation and transfer efficiency of electron-hole pairs in PFCN2 composite are remarkably enhanced by the P25-g-C_3N_4 heterojunction structure and uniform metal doping. The photocatalytic efficiencies of the composites may be promoted owing to the improved photogenerated charge mobility. The results are also consistent with the photocatalytic activity above and help to propose the photodegradation mechanism of the modified photocatalysts.

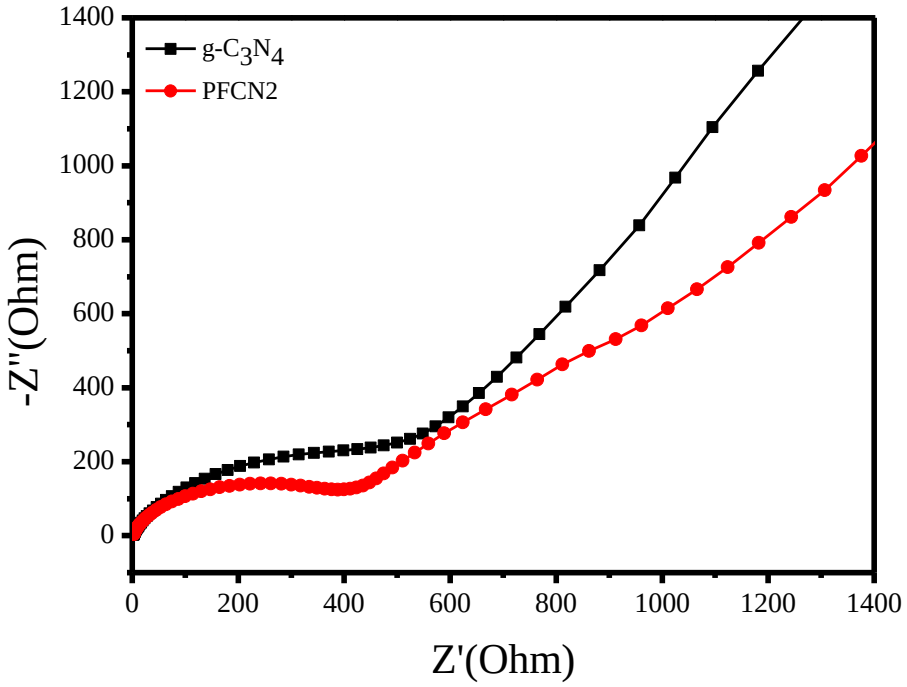

Figure 7. EIS Nyquist plots of g-C_3N_4 and Fe-CN-P25 photocatalysts under visible light irradiation.

3.8. Discussion on photocatalytic mechanism of Fe-CN-P25 composites.

The mechanism of visible-light photocatalytic enhancement proposed here is based on the physicochemical and photocatalytic properties of modified composites (Fig. 8). As is well-known, g-C_3N_4 versus TiO_2 has lower conduction band (CB) edge potential (-1.21 vs. -0.29 eV) and lower valence band (VB) edge potential (+1.51 vs. +2.91 eV). Therefore, when the modified composites were irradiated with visible light, g-C_3N_4 could absorb visible light to form electron-hole pairs, but TiO_2 was barely excited. Moreover, the photogenerated electrons of g-C_3N_4 tend to transfer to TiO_2 via their heterojunction interfaces, while the photoinduced holes stay at g-C_3N_4. Meanwhile, the Fe^{3+} doping in the composites could broaden the absorption range and thus improve the electron-hole generation efficiency, which prolongs the lifetime of the charge carriers and decelerates the electron-hole recombination. Moreover, the transferred electrons on the CB of TiO_2 could motivate the reduction from toxic Cr(VI) to nontoxic Cr(Ⅲ), while the photoinduced holes remaining in g-C_3N_4 would participate in oxidizing the dyes to CO_2, H_2O and other harmless products[30]. As a result, the modified composites exhibit higher visible-light photocatalytic activity than pure P25 and g-C_3N_4.

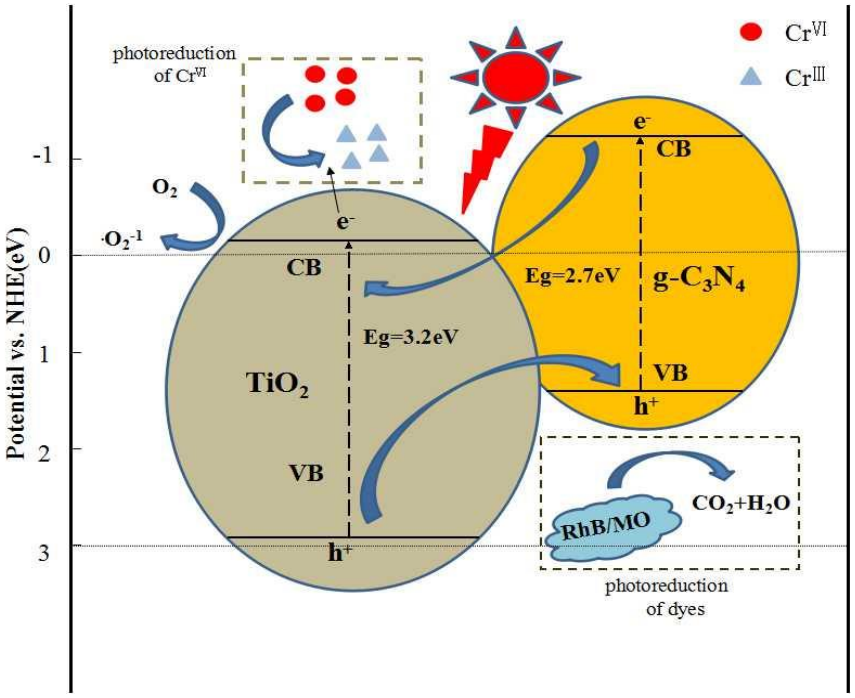

Figure 8. Scheme of proposed possible mechanism of dyes and Cr(VI) photodegradation by the Fe-CN-P25 composites under visible-light irradiation.

4. CONCLUSIONS

g-C_3N_4 and Fe ions co-modified P25 TiO_2 photocatalysts were prepared through a simple facile route. XPS and FT-IR confirmed the presence of g-C_3N_4 and metal ions in the heterojunction catalysts. TEM showed the g-C_3N_4 coating layers with average monolayer thickness of 0.36 nm could enhance the visible light absorption, as indicated from UV-vis DRS. The photocatalysts showed significant enhancement in photodegradation of RhB, MO and Cr(VI) under visible-light irradiation, while the excellent cycle stability was also confirmed. Furthermore, the composite synthesized with 5g melamine and 2 wt.% metal showed the optimal photocatalytic activity. EIS indicated the modified composite was effective in separation of photoinduced electron-hole pairs. The enhanced photocatalytic activity was mainly attributed to the formation of g-C_3N_4/P25 heterojunction and the doping of Fe ions, which decelerate the recombination of electron-hole and efficiently improve the separation and transfer of photogenerated charge carriers.

ACKNOWLEDGEMENTS
This work was financially supported by the National Science Foundation of China (Grant No.61171008 and 51502172), Shanghai Jubo Energy Technology Co., Ltd and Yancheng Huanbo Energy Technology Co., Ltd.

References

1. H. L. Wang, L. S. Zhang, Z. G. Chen, J. Q. Hu, S. J. Li, Z. H. Wang, J. S. Liu and X. C. Wang, *Chem. Soc. Rev.*, 43 (2014) 5234.

2. C. Chen, W. Ma and J. Zhao, *Chem. Soc. Rev.*, 39 (2010) 4206.
3. S. C. Yan, Z. S. Li, and Z. G. Zou, *Langmuir.*, 25 (2009) 10397.
4. Y. L. Li, J. S. Wang, Y. L. Yang, Y. Zhang, D. He, Q. E. An and G. Z. Cao, *J. Hazard. Mater.*, 292 (2015) 79.
5. X. X. Yang, H. Y. Huang, M. Kubota, Z. H. He, N. Kobayashi, X. S. Zhou, B. Jin and J. Luo, *Mater. Res. Bull.*, 76 (2016) 79.
6. Z. A. Lan, G. G. Zhang, and X. C. Wang, *Appl. Catal. B-Environ.*, 192 (2016) 116.
7. X. Liu, N. Chen, Y. X. Li, D. Y. Deng, X. X. Xing and Y. D. Wang, *Sci. Rep.*, 6 (2016) 39531.
8. R. Mohini and N. Lakshminarasimhan, *Mater. Res. Bull.*, 76 (2016) 370.
9. X. Song, Y. Hu, M. M. Zheng and C. H. Wei, *Appl. Catal. B-Environ.*, 182 (2016) 587.
10. S. Ghasemi, S. Rahimnejad, S. R. Setayesh, S. Rohani and M. R. Gholami, *J. Hazard. Mater.*, 172 (2009) 1573.
11. A. Busiakiewicz, A. Kisielewska, I. Piwonski and D. Batory, *Appl. Surf. Sci.*, 401 (2017) 378.
12. X. C. Wang, X. F. Chen, A. Thomas, X. Z. Fu and M. Antonietti, *Adv. Mater.*, 21 (2009) 1609.
13. X. P. Wang, Y. X. Tang, M. Y. Leiw and T. T. Lim, *Appl. Catal. A-Gen.*, 409 (2011) 257.
14. Y. M. Wu, L. Tao, J. Zhao, X. Yue, W. Y. Deng, Y. X. Li and C. Y. Wang, *Res. Chem. Intermed.*, 42 (2016) 3609.
15. Y. P. Zang, L. P. Li, Y. S. Xu, Y. Zuo and G. S. Li, *J. Mater. Chem. A.*, 2 (2014) 15774.
16. S. F. Kang, Y. Fang, Y. K. Huang, L. F. Cui, Y. Z. Wang, H. F. Qin, Y. M. Zhang, X. Li and Y. G. Wang, *Appl. Catal. B-Environ.*, 168 (2015) 472.
17. L. W. Zhang, H. B. Fu and Y. F. Zhu, *Adv. Funct. Mater.*, 18 (2008) 2180.
18. J. H. Li, Y. L. Liu, H. M. Li and C. Chen, *J. Photochem. Photobiol. A.*, 317 (2016) 151.
19. J. Z. Ma, C. X. Wang, and H. He, *Appl. Catal. B-Environ.*, 184 (2016) 28.
20. Z. F. Jiang, C. Z. Zhu, W. M. Wan, K. Qian and J. M. Xie, *J. Mater. Chem. A.*, 4 (2016) 1806.
21. J.L. Jia, D. Li, J.F. Wan and X.J. Yu, *J. Ind. Eng. Chem.*, 33 (2016) 162.
22. W. Li, C. Li, B. Chen, X. L. Jiao and D. R. Chen, *Rsc Adv.*, 5 (2015) 34281.
23. J. Y. Lei, Y. Chen, F. Shen, L. Z. Wang, Y. D. Liu and J. L. Zhang, *J. Alloys Compd.*, 631 (2015) 328.
24. X. J. Bai, R. L. Zong, C. X. Li, D. Liu, Y. F. Liu and Y. F. Zhu, *Appl. Catal. B-Environ.*, 147 (2014) 82.
25. R. R.Hao, G. H. Wang, H. Tang, L. L. Sun, C. Xu and D. Y. Han, *Appl. Catal. B-Environ.*, 187 (2016) 47.
26. S. Z. Hu, R. R. Jin, G. Lu, D. Liu and J. Z. Gui, *Rsc Adv.*, 4 (2014) 24863.
27. T. Sano, K. Koike, T. Hori, T. Hirakawa, Y. Ohko and K. Takeuchi, *Appl. Catal. B-Environ.*, 198 (2016) 133.
28. J. F. Guo, B. W. Ma, A. Y. Yin, K. N. Fan and W. L. Dai, *J. Hazard. Mater.*, 211 (2012) 77.
29. X. L. Yang, F. F. Qian, G. J. Zou, M. L. Li, J. R. Lu, Y. M. Li and M. T. Bao, *Appl. Catal. B-Environ.*, 193 (2016) 22.
30. N. Wang, L. H. Zhu, K. J. Deng, Y. B. She, Y. M. Yu and H. Q. Tang, *Appl. Catal. B-Environ.*, 95 (2010) 400.